Comparison of Mathematical Models for the HUGIN 4500 AUV Based on Experimental Data

Øyvind Hegrenæs
Department of Engineering Cybernetics,
Norwegian University of Science and Technology, NO-7491 Trondheim, Norway

Oddvar Hallingstad
Department of Engineering Cybernetics,
Norwegian University of Science and Technology, NO-7491 Trondheim, Norway

Bjørn Jalving
Kongsberg Maritime, NO-3191 Horten, Norway

***Abstract*—This paper reports the development and comparison of several mathematical models for describing the response of the HUGIN 4500 AUV as a function of measured actuator inputs. As a crucial step in fitting the derived models to experimental field data, a combination of dedicated experiments and least-squares estimation is applied in order to obtain an estimate of the sea current, and properly compensate for it during the identification stage. The established models are extensively cross-validated with uncorrelated data, which is a standard step in system identification to prevent over-fitting observed data. The vehicle response predicted by the proposed models shows good agreement with real measurements. The possible use of mathematical vehicle models includes control and navigation system design, applications to fault detection and integrity, and vehicle design evaluation. The content of this paper is motivated from the perspective of developing second generation underwater navigation systems, tightly integrating model-based velocity estimates and knowledge of commanded and measured actuator signals.**

I. Introduction

Deciding which sensor outfit to include in an underwater navigation system is important both from a performance and cost perspective. A typical sensor outfit consists of standard components such as magnetic compass, pressure and orientation sensors, and some class of inertial navigation system (INS). In addition, various sources of position aiding may be available, for instance long baseline (LBL) or ultra short baseline (USBL) acoustics, geophysical or terrain-based techniques, and surface GPS.

In practice, a submerged underwater vehicle does not have continuous position updates, hence a navigation solution based solely on INS, and especially low-cost INS, will have an unacceptable position error drift without additional aiding. While most high-end systems incorporate a Doppler velocity log (DVL) in their sensor suite in order to limit the drift, this additional expense is not always feasible for low-cost systems. Even when a DVL unit is included, situations may also occur where it fails to work or measurements are discarded due to decreased quality. In either case, in the absence of DVL measurements, alternative velocity information is required to achieve an acceptable low drift navigation solution between position updates. One possibility is to utilize mathematical vehicle models.

The purpose of this paper is twofold. First, from an underwater navigation point of view and with the aim of providing model-based velocity estimates, suitable models for describing the vehicle response are developed based on open water propulsion characteristics and free swimming sea trial data. As part of this work, a combination of dedicated experiments and least-squares estimation is applied in order to obtain an estimate of the sea current, and properly compensate for it during model development and identification. Second, an analysis is given where the performances of the derived models are compared, including their short-term and long-term error propagation.

This paper is organized as follows. Section I-A and I-B give a historical recap and review of both early and recent work related to modeling of underwater vehicles. Section II reports the derivation of the mathematical models investigated in this paper. The identification stage is described in Section III, including an outline of the procedures used for estimating and compensating for current. Section IV and V describe the experimental setup and experimental results.

A. Dynamical Modeling of Underwater Vehicles

From a historical perspective, the study of a solid's motion through a liquid is commonly attributed to the early work by Sir Horace Lamb, originally published in 1879 and later reissued in numerous editions. As stated in [1], the development of the subject should also partly be credited to [2]. By treating the solid and the inviscid fluid as one dynamical system, and by exploiting its kinetic energy, the work by Lamb and Kirchhoff resulted in what is today denoted as added mass. Their approach was later adapted by researchers at the U.S. David Taylor Model Basin (DTMB) in the 1950s and 1960s, as reported in [3].

While primarily dealing with surface ships moving in the horizontal plane, most of the early contributions can be generalized to submersibles as well. A proposal was made by [4] to model a vehicle as a rigid body moving in three degrees of freedom (DOF) under the influence of external forces and moments. Their assertion was based on Newton's second law, resulting in an Earth-fixed representation. It was later found more convenient to represent the equations of motion in a body-fixed reference frame, with the origin placed in the center of gravity (CG) of the ship. With the motivation of exploiting vehicle geometrical symmetries, it was suggested in [5] to develop the equations of motion for an axis-system parallel to the principle axis of inertia through CG, but with the origin not necessarily in

CG. Today, this convention, and the notion of representing a submersible as a rigid body subject to external forces and moments, form the fundamental basis of most models.

Even when considered as a rigid body, an exact analysis of the external forces and moments is only possible by including the underlaying infinite-dimensional dynamics of the surrounding fluid. While this can be done using partial differential equations (PDEs), it still involves a formidable computational burden, infeasible for most practical applications. As a result, the conventional approach has been to use various finite-dimensional approximations.

With their foresight to follow aviation practice, it was advocated by [4] that similar techniques could be applied for describing the external forces and moments acting on a marine vehicle. According to [6], the work by Davidson and Schiff can be traced back to [7], confirming the close resemblance between modeling of aerial and naval crafts. While the linear representation in [4] is justified in the low velocity regime, it turns out that many of the external forces and moments become nonlinear for sufficiently large velocities and velocity products. For most underwater vehicles this is certainly the case for operations resulting in high sideslip angles or high angles of attack. In attempt to resolve this issue, [5] proposed to use a truncated Taylor series expansion for describing the nonlinear external forces and moments acting on the vehicle. The approach, which can also be used for developing a linear representation, exploits properties of even and odd functions for selecting the zero terms of the Taylor series. Another nonlinear representation called the second order modulus was proposed by [8] where, as apposed to cubic terms in the Taylor series approach, the nonlinearities are accounted for by introducing several modulus terms. As discussed in [6], the two different approaches have slightly different properties. In [9], [10], the second order modulus approach is used for representing the hydrodynamic viscous damping, while both representations are combined in [11] since that gave the best fit to real data. A complete and widely accepted representation for describing the motion of submarines is given in [12], and in revised form in [13]. Details on the derivations are unfortunately not included.

Common for the above mentioned representations is the need for so-called hydrodynamics derivatives. These are coefficients that quantify the forces and moments on the vehicle as a function of its attitude and motion. An alternative approach is the component buildup method [14], [15], [16]. With this method, the external forces and moments on the vehicle are derived from empirical relationships which only require specification of the vehicle geometry. Each component of the vehicle is modeled separately using simple hydrodynamic relationships. The contributions from each component are then summed together to provide the total forces and moments acting on the submersible.

Clearly, a one-to-one comparison of different models is not straightforward, and the forces and moments acting on a submerged vehicle are strongly dependent on the geometry of the vehicle, and also by the environment in which it operates. For a further discussion on modeling of ships and underwater vehicles the reader may refer to [17], [18], [9], [10], [19], [20], [21], and references therein.

B. Application of Dynamic Vehicle Models

Besides the obvious use as a simulation aid, approximate finite-dimensional models of underwater vehicles have successfully been applied in numerous control system designs, e.g. [22], [23], [24], [25]. Model-based fault detection is another active field of research, with several applications in industry, automotive and aviation. For underwater applications, vehicle models have only recently been used for detecting faults in the control system [26], [27], [28]. With focus on underwater navigation and integrity, vehicle models are used in [29] in order to detect faults in an aided navigation system. The possible use of models for outlier filtering in hydro-acoustic positioning is also discussed.

To date, the development and implementation of model-based state estimators for underwater vehicle navigation has primarily focused on applying various Kalman filters to purely kinematic models. Fewer papers report kinetic model-based estimators or observers [30], [31].

II. Modeling

This section describes the derivation of the mathematical models examined in this paper. Only motion in the horizontal plane is considered, hence neglecting coupling from heave, roll, and pitch. We assume the presence of a constant or slowly varying current whose magnitude and direction is measured or estimated. In this paper, suitable estimates are obtained according to Section III-A. It is furthermore assumed that the current is irrotational and two-dimensional, and that the vehicle operates in a uniform unbounded fluid, hence neglecting boundary effects.

A. Notation and Preliminaries

In cases where a vehicle operates in a limited geographical area, it is usually sufficient to use a local flat Earth approximation when describing its location. Let $\{m\}$ denote an Earth-fixed coordinate frame, which for our purposes is considered inertial. The origin is located at the surface of the WGS-84 Earth ellipsoid, and the orientation is north-east-down (NED). Similarly, let $\{w\}$ denote a reference frame where the origin is fixed to, and translates with the water (due to current). Since the current is irrotational by assumption, $\{w\}$ does not rotate relative to $\{m\}$. The last frame $\{b\}$ is a body-fixed reference frame where the axes coincide with the principal axes of the vehicle. The origin is placed at the vehicle center of buoyancy. A general expression of the vehicle position can now be written as

$$\begin{aligned} \boldsymbol{p}^m_{mb} &= \boldsymbol{p}^m_{mw} + \boldsymbol{p}^m_{wb} \\ &= \boldsymbol{p}^m_{mw} + \boldsymbol{R}^m_w \boldsymbol{p}^w_{wb}, \end{aligned} \tag{1}$$

where $\boldsymbol{p}^m_{wb} \in \mathbb{R}^3$ is the vector from the origin of $\{w\}$ to the origin $\{b\}$, decomposed in $\{m\}$, and $\boldsymbol{R}^m_w \in SO(3)$ is the rotation matrix from $\{m\}$ to $\{w\}$, or equally, the transformation matrix from $\{w\}$ to $\{m\}$. The velocity of $\{b\}$ relative to $\{m\}$, represented in $\{m\}$, is given as $\boldsymbol{v}^m_{mb} := \dot{\boldsymbol{p}}^m_{mb}$, or decomposed in $\{b\}$ as $\boldsymbol{v}^b_{mb} := \boldsymbol{R}^b_m \boldsymbol{v}^m_{mb}$. The interpretation of the other variables follows directly. Taking the time derivative of both sides of (1) yields

$$\begin{aligned} \dot{\boldsymbol{p}}^m_{mb} &= \dot{\boldsymbol{p}}^m_{mw} + \dot{\boldsymbol{R}}^m_w \boldsymbol{p}^w_{wb} + \boldsymbol{R}^m_w \dot{\boldsymbol{p}}^w_{wb} \\ &= \dot{\boldsymbol{p}}^m_{mw} + \boldsymbol{R}^m_w \dot{\boldsymbol{p}}^w_{wb}, \end{aligned} \tag{2}$$

TABLE I
NOMENCLATURE

Description	Variable	Entries*
Vehicle position (cartesian)	$\boldsymbol{p}^m_{mb}$	(x, y, z)
Earth-fixed linear velocity	$\boldsymbol{v}^b_{mb}$	(u, v, w)
Water relative linear velocity	$\boldsymbol{v}^b_{wb}$	(u_r, v_r, w_r)
Current velocity	$\boldsymbol{v}^b_{mw}$	(u_c, v_c, w_c)
Current velocity	$\boldsymbol{v}^m_{mw}$	(u^m_c, v^m_c, w^m_c)
Vehicle angular velocity	$\boldsymbol{\omega}^b_{mb}$	(p, q, r)
External forces on vehicle	$\boldsymbol{f}^b$	(X, Y, Z)
External moments on vehicle	$\boldsymbol{m}^b$	(K, M, N)
Attitude (roll, pitch, yaw)	$\boldsymbol{\Theta}$	(ϕ, θ, ψ)

* Based on SNAME notation

where $\dot{\boldsymbol{R}}^m_w$ equals zero due to the assumption of irrotational current. Substituting for the derivatives, and multiplying both sides of (2) with $\boldsymbol{R}^b_m$ gives the velocity relationship

$$\boldsymbol{v}^b_{mb} = \boldsymbol{R}^b_m \boldsymbol{v}^m_{mw} + \boldsymbol{v}^b_{wb}. \tag{3}$$

Analogous to the linear velocities, their angular counterparts are given as $\boldsymbol{\omega}^m_{mb}$ and $\boldsymbol{\omega}^b_{mb} := \boldsymbol{R}^b_m \boldsymbol{\omega}^m_{mb}$. Note that if yaw-pitch-roll (ψ, θ, ϕ) type Euler angles are used for describing the vehicle attitude, and hence the parametrization of $\boldsymbol{R}^m_b$, then the change rates of the same angles are related to $\boldsymbol{\omega}^b_{mb}$ through a linear transformation given in [10].

Taking the time derivative of both sides of (3) gives

$$\begin{aligned} \dot{\boldsymbol{v}}^b_{mb} &= \dot{\boldsymbol{R}}^b_m \boldsymbol{v}^m_{mw} + \boldsymbol{R}^b_m \dot{\boldsymbol{v}}^m_{mw} + \dot{\boldsymbol{v}}^b_{wb} \\ &= \dot{\boldsymbol{R}}^b_m \boldsymbol{v}^m_{mw} + \dot{\boldsymbol{v}}^b_{wb}, \end{aligned} \tag{4}$$

where the assumption of a constant or slowly varying current implies $\dot{\boldsymbol{v}}^m_{mw} \approx \boldsymbol{0}$. From (4) and from the rule of time differentiation of rotation matrices [32] we get that

$$\begin{aligned} \dot{\boldsymbol{v}}^b_{mb} &= \dot{\boldsymbol{v}}^b_{wb} + \boldsymbol{S}(\boldsymbol{\omega}^b_{bm}) \boldsymbol{R}^b_m \boldsymbol{v}^m_{mw} \\ &= \dot{\boldsymbol{v}}^b_{wb} - \boldsymbol{S}(\boldsymbol{\omega}^b_{mb}) \boldsymbol{R}^b_m \boldsymbol{v}^m_{mw}, \end{aligned} \tag{5}$$

where $\boldsymbol{S}(\cdot)$ is a skew-symmetric matrix. Notice that (5) implies that $\dot{\boldsymbol{v}}^b_{mb} \approx \dot{\boldsymbol{v}}^b_{wb}$ for small $\boldsymbol{\omega}^b_{mb}$. For motion in the horizontal plane, this is equivalent to low yaw rates. Finally note that $\boldsymbol{\omega}^b_{mb} = \boldsymbol{\omega}^b_{wb}$, since $\boldsymbol{\omega}^b_{mw}$ is zero by assumption.

The correspondence between the variables above and the commonly used notation established by The Society of Naval Architects and Marine Engineers (SNAME) [33] is shown in Table I. An illustration showing the different speed entities along the body x-axis is shown in Fig. 1.

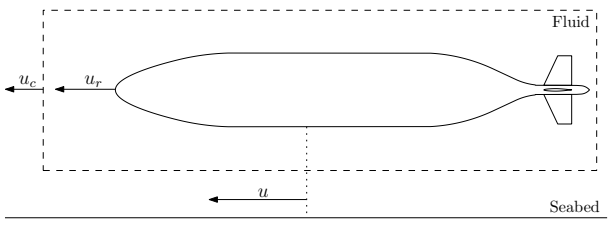

Fig. 1. Water relative vehicle speed u_r, current speed u_c, and Earth-fixed vehicle speed u. Profile of the HUGIN 4500 AUV used as illustration.

B. The 3 DOF maneuvering model

As shown in [10], a general expression of the rigid body equations of motion can be written in compact form as

$$\boldsymbol{M}_{RB}\dot{\boldsymbol{\nu}} + \boldsymbol{C}_{RB}(\boldsymbol{\nu})\boldsymbol{\nu} = \boldsymbol{\tau}_{RB}, \tag{6}$$

where $\boldsymbol{M}_{RB}$ is the rigid body inertia matrix, $\boldsymbol{C}_{RB}$ is the corresponding matrix of Coriolis and centripetal terms, and $\boldsymbol{\tau}_{RB}$ is a generalized force vector of external forces and moments. For 3 DOF motion in the horizontal plane (surge, sway, and yaw), the generalized force and velocity vectors are $\boldsymbol{\tau}_{RB} = [X, Y, N]^\top$ and $\boldsymbol{\nu} = [u, v, r]^\top$, respectively. If the vector from the origin of $\{b\}$ to the vehicle center of gravity is given as $\boldsymbol{r}_g = [0, 0, z_g]^\top$, then it is found that

$$\boldsymbol{M}_{RB} = \begin{bmatrix} m & 0 & 0 \\ 0 & m & 0 \\ 0 & 0 & I_z \end{bmatrix} \quad \boldsymbol{C}_{RB} = \begin{bmatrix} 0 & 0 & -mv \\ 0 & 0 & mu \\ mv & -mu & 0 \end{bmatrix},$$

where m is the mass of the vehicle in water and I_z is the vehicle moment of inertia about the z-axis of $\{b\}$.

As mentioned, the ambiguity in modeling an underwater vehicle arises when expressing the right hand-side of (6). One possibility is to linearly superimpose $\boldsymbol{\tau}_{RB}$ as follows

$$\boldsymbol{\tau}_{RB} = \boldsymbol{\tau}_S + \boldsymbol{\tau}_H + \boldsymbol{\tau}, \tag{7}$$

where the generalized hydrostatic force $\boldsymbol{\tau}_S$ is known in its exact form. The generalized hydrodynamic force $\boldsymbol{\tau}_H$ arise from the reaction of the surrounding fluid to the vehicle motion. It is in the evaluation of $\boldsymbol{\tau}_H$ that the greatest source of uncertainty lies, due to the fact that one is adopting a finite-dimensional approximation to the underlaying infinite-dimensional dynamics of the fluid. The hydrodynamics can be broadly categorized under two groups, where one involves the motion of the vehicle in an ideal or inviscid fluid, and the other is due to fluid viscosity effects. By letting $\boldsymbol{\tau}_I$ and $\boldsymbol{\tau}_R$ denote the generalized ideal and real (viscous) fluid forces, we can write $\boldsymbol{\tau}_H = \boldsymbol{\tau}_I + \boldsymbol{\tau}_R$.

The last component, $\boldsymbol{\tau} = \boldsymbol{\tau}_P + \boldsymbol{\tau}_C$, consists of forces and moments from propulsion, and from the control surfaces.

The profile of the HUGIN 4500 AUV is shown in Fig. 1. The bare hull is a body of revolution, and the cruciform tail configuration is top-bottom, port-starboard symmetric. A general 3 DOF model for this vehicle can be written as

$$\begin{aligned} \boldsymbol{M}_{RB}\dot{\boldsymbol{\nu}} + \boldsymbol{C}_{RB}(\boldsymbol{\nu})\boldsymbol{\nu} = \boldsymbol{\tau} - \boldsymbol{M}_A\dot{\boldsymbol{\nu}}_r - \boldsymbol{C}_A(\boldsymbol{\nu}_r)\boldsymbol{\nu}_r - \\ \boldsymbol{d}(\boldsymbol{\nu}_r)\boldsymbol{\nu}_r - \boldsymbol{l}(\boldsymbol{\nu}_r) - \boldsymbol{g}(\boldsymbol{\Theta}), \end{aligned} \tag{8}$$

where $\boldsymbol{d}(\boldsymbol{\nu}_r) = \boldsymbol{D}_L + \boldsymbol{D}_{NL} + \boldsymbol{D}_T$ and $\boldsymbol{\nu}_r = [u_r, v_r, r]^\top$. The terms in (8) and some of their properties are:

1) $\boldsymbol{M}_A$ accounts for added mass and moment of inertia. Similarly, $\boldsymbol{C}_A$ accounts for added Coriolis and centripetal terms. Both contribute to $\boldsymbol{\tau}_I$.

$$\boldsymbol{M}_A = \begin{bmatrix} -X_{\dot{u}} & 0 & 0 \\ 0 & -Y_{\dot{v}} & -Y_{\dot{r}} \\ 0 & -N_{\dot{v}} & -N_{\dot{r}} \end{bmatrix}$$

$$\boldsymbol{C}_A = \begin{bmatrix} 0 & 0 & Y_{\dot{r}}r + Y_{\dot{v}}v_r \\ 0 & 0 & -X_{\dot{u}}u_r \\ -Y_{\dot{r}}r - Y_{\dot{v}}v_r & X_{\dot{u}}u_r & 0 \end{bmatrix}$$

2) $\boldsymbol{D}_L$ and $\boldsymbol{D}_{NL}$ represent linear and nonlinear hydrodynamic damping. $\boldsymbol{D}_L$ typically accounts for linear skin friction, while $\boldsymbol{D}_{NL}$ is caused by turbulent skin

friction and vortex shedding. Both contribute to $\boldsymbol{\tau}_R$.

$$\boldsymbol{D}_L = \begin{bmatrix} -X_u & 0 & 0 \\ 0 & -Y_v & -Y_r \\ 0 & -N_v & -N_r \end{bmatrix}$$

$$\boldsymbol{D}_{NL} = \begin{bmatrix} -X_{|u|u}|u_r| & 0 & 0 \\ 0 & -Y_{|v|v}|v_r| & -Y_{|r|r}|r| \\ 0 & -N_{|v|v}|v_r| & -N_{|r|r}|r| \end{bmatrix}$$

3) $\boldsymbol{D}_T$ represents forces and moment resulting from a truncated Taylor series expansion. Contributes to $\boldsymbol{\tau}_R$.

$$\boldsymbol{D}_T = \begin{bmatrix} 0 & -X_{vr}r - X_{vv}v_r & -X_{rr}r \\ 0 & 0 & 0 \\ 0 & 0 & 0 \end{bmatrix}$$

4) Forces and moment from body lift are represented by $\boldsymbol{l}$, and are due to the vehicle motion through water at an angle of attack (sideslip in the horizontal plane). Valid for small sideslip angles. Contributes to $\boldsymbol{\tau}_I$.

$$\boldsymbol{l} = \begin{bmatrix} 0 \\ -Y_{uv_b}u_r v_r \\ -N_{uv_b}u_r v_r \end{bmatrix}$$

5) Contribution from gravity and buoyancy. W and B denote weight and buoyancy. Contributes to $\boldsymbol{\tau}_S$.

$$\boldsymbol{g} = \begin{bmatrix} (W-B)\sin(\theta) \\ -(W-B)\cos(\theta)\sin(\phi) \\ 0 \end{bmatrix}$$

6) Forces and moment produced by the control surfaces. The deflections of the top and bottom rudder are denoted δr_t and δr_b. Similarly, δs_p and δs_s for port and starboard stern plane. Contributes to $\boldsymbol{\tau}$.

$$\boldsymbol{\tau}_C = \begin{bmatrix} X_{\delta\delta uu}(\delta r_t^2 + \delta r_b^2 + \delta s_p^2 + \delta s_s^2)u_r^2 \\ Y_{\delta uu}(\delta r_t + \delta r_b)u_r^2 + Y_{ur_\delta}u_r r + Y_{uv_\delta}u_r v_r \\ N_{\delta uu}(\delta r_t + \delta r_b)u_r^2 + N_{ur_\delta}u_r r + N_{uv_\delta}u_r v_r \end{bmatrix}$$

7) Forces (thrust) and moment produced by the propeller mounted at the aft. The propeller rotation rate is given in rounds per second, and is denoted by n. w is the wake fraction number. Contributes to $\boldsymbol{\tau}$.

$$\boldsymbol{\tau}_P = \begin{bmatrix} T_{|n|n}|n|n + T_{|n|u}|n|(1-\mathrm{w})u_r \\ 0 \\ 0 \end{bmatrix}$$

The coefficients $X_{(\cdot)}, Y_{(\cdot)}$ and $N_{(\cdot)}$ are called hydrodynamic derivatives because they are the partial derivatives of the forces and moments with respect to the corresponding velocities or control surface deflections, e.g. $Y_r := \frac{\partial Y}{\partial r}$. This is in agreement with [33]. The propulsion coefficients $T_{(\cdot)}$ are typically found from open-water propulsion tests.

For (8) one must decide upon using the relative velocity $\boldsymbol{\nu}_r$ or the inertial velocity $\boldsymbol{\nu}$ as the velocity state. The current velocity must in either case be measured or estimated. Recall the relationships in (3) and (5). Under the assumption that $\dot{\boldsymbol{\nu}} \approx \dot{\boldsymbol{\nu}}_r$, the final model can be written as

$$\boldsymbol{M}\dot{\boldsymbol{\nu}}_r = \boldsymbol{\tau} - \boldsymbol{C}(\boldsymbol{\nu}, \boldsymbol{\nu}_r) - \boldsymbol{d}(\boldsymbol{\nu}_r)\boldsymbol{\nu}_r - \boldsymbol{l}(\boldsymbol{\nu}_r) - \boldsymbol{g}(\boldsymbol{\Theta}), \quad (9)$$

where

$$\boldsymbol{M} := \boldsymbol{M}_{RB} + \boldsymbol{M}_A$$
$$\boldsymbol{C}(\boldsymbol{\nu}, \boldsymbol{\nu}_r) := \boldsymbol{C}_{RB}(\boldsymbol{\nu})\boldsymbol{\nu} + \boldsymbol{C}_A(\boldsymbol{\nu}_r)\boldsymbol{\nu}_r.$$

C. The 1 DOF surge model

A survey type AUV like the HUGIN 4500 typically navigates according to a predetermined mission plan. For instance, a lawn mower pattern effectively cancels out slowly varying errors in velocity and heading, and the vehicle is relatively quickly able to survey a large geographical area. Evidently, such a pattern implies that the dominating trajectories are the straight lines between successive turns, and it follows that surge is the significant velocity component when the vehicle sideslip and angle of attack are small. Motivated by this discussion, two alternative 1 DOF surge models are given subsequently.

A physical model can be deduced from (9) by assuming that $v_r \approx 0$ and $r \approx 0$. The resulting model is given as

$$(m - X_{\dot{u}})\dot{u}_r = \tau + X_u u_r + X_{|u|u}|u_r|u_r - g, \quad (10)$$

where $\tau = \tau_p + \tau_c$ and

$$\tau_p = T_{|n|n}|n|n + T_{|n|u}|n|(1-\mathrm{w})u_r$$
$$\tau_c = X_{\delta\delta uu}(\delta r_t^2 + \delta r_b^2 + \delta s_p^2 + \delta s_s^2)u_r^2$$
$$g = (W-B)\sin(\theta).$$

For most cases HUGIN 4500 operates without speed control (on u). If n is constant or few set-point changes are commanded, the vehicle is properly ballasted, and the control surface deflections are small, it can be argued that the complexity of (10) is not justified. An alternative may be to implement a simple static model as a table look-up, based on experimental data, that is,

$$u_r = f(n_s), \quad (11)$$

where n_s is the is the control system set-point for n. A similar approach can be used for establishing an expression for v_r. It is emphasized that a 1 DOF surge model is not able to predict the transients during a turn maneuver.

D. Discussion

As mentioned, a comparison of different mathematical vehicle models is not straightforward. Some parts are however standard, such as (6) and $\boldsymbol{\tau}_S$ in (7). In addition, the components of $\boldsymbol{\tau}_I$ resulting from added mass effects are well understood, as are the forces and moments produced by the propulsion system and the control surfaces. The expressions related to the fins were derived based on the component build-up method, and with the assumption that the fins do not stall regardless of angle of attack. A bilinear thrust model [10] was used for the propulsion system. Note that more sophisticated models do exist [34], [35], [21], [36]. The components of $\boldsymbol{\tau}_I$ resulting from lift on the hull were derived based on potential theory [37], [38]. Potential theory is limited to angles of attack near zero, where viscous effects are small. At higher angles the viscous part becomes increasingly important, and should be taken into account [15]. As for the real hydrodynamic fluid force $\boldsymbol{\tau}_R$, there is no standard procedure for describing these components. At the end, what decides in practise is often the representation which gives the most realistic fit to data.

The assumption $\dot{\boldsymbol{v}}^b_{mb} \approx \dot{\boldsymbol{v}}^b_{wb}$ in (5) is clearly valid for small $\boldsymbol{\omega}^b_{mb}$ and moderate current speeds. It is indeed

satisfied for normal operations with HUGIN 4500 (including turning maneuvers). Current speeds at the test site considered in this paper were found to be in the order of 0-3 cm/s. For a general vehicle and survey area however, great care must be shown since the assertion may not always hold. Note also that $\dot{\boldsymbol{v}}_{mb}^b$ in (5) is not a standard acceleration, since it is derived from a position vector first differentiated relative to $\{m\}$, then relative to $\{b\}$. What it describes is how the velocity vector changes as seen from $\{b\}$, typically varying around zero for most vehicles.

III. Current Estimation and Parameter Identification

The derived vehicle models from the previous section contain unknown parameters for which values need to be estimated. The values have to be chosen carefully to adequately represent the behavior of the AUV. A description of the parameter identification stage is given below.

A. Current Estimation and Compensation

Prior to identifying the model coefficients it is necessary to obtain an estimate of the sea current, and thereafter, an estimate of the water relative velocity of the vehicle. This must be done since HUGIN 4500 currently does not measure this velocity directly. It was shown in [39] that the current can be estimated by utilizing the measured attitude and Earth-fixed velocity of the vehicle. The following summary is based on the results in the same reference.

The expression in (3) is general and also valid when the entries of $\boldsymbol{v}_{mw}^m$ are all non-zero. As noted earlier however, it is assumed throughout this paper that the vertical current component, or equally, the third entry of $\boldsymbol{v}_{mw}^m$ is zero at all time. Based on this assertion we can rewrite (3) as

$$\boldsymbol{v}_{mb}^b = \begin{bmatrix} \boldsymbol{c}_1 & \boldsymbol{c}_2 \end{bmatrix} \begin{bmatrix} u_c^m \\ v_c^m \end{bmatrix} + \boldsymbol{v}_{wb}^b, \tag{12}$$

where $\boldsymbol{c}_i$ denotes the i-th column of the rotation matrix $\boldsymbol{R}_m^b$. Now, by defining $\boldsymbol{z} := \boldsymbol{v}_{mb}^b$, we have from (12) that

$$\underbrace{\begin{bmatrix} \boldsymbol{z}(t_1) \\ \boldsymbol{z}(t_2) \\ \vdots \\ \boldsymbol{z}(t_N) \end{bmatrix}}_{\boldsymbol{Z} \in \mathbb{R}^{3N \times 1}} = \underbrace{\begin{bmatrix} \boldsymbol{I}_{3\times 3} & \boldsymbol{c}_1(t_1) & \boldsymbol{c}_2(t_1) \\ \boldsymbol{I}_{3\times 3} & \boldsymbol{c}_1(t_2) & \boldsymbol{c}_2(t_2) \\ \vdots & \vdots & \vdots \\ \boldsymbol{I}_{3\times 3} & \boldsymbol{c}_1(t_N) & \boldsymbol{c}_2(t_N) \end{bmatrix}}_{\boldsymbol{H} \in \mathbb{R}^{3N \times 5}} \boldsymbol{\theta}, \tag{13}$$

where $\boldsymbol{\theta} = [u_r, v_r, w_r, u_c^m, v_c^m]^\top \in \mathbb{R}^5$, N is the number of samples, and $t_1, t_2, \ldots, t_N$ represent the sample times. The sample times do not have to be uniformly spaced. The total duration time given as $t_N - t_1$ should however not be too long since this may violate the assumption that $\dot{\boldsymbol{v}}_{mw}^m = \boldsymbol{0}$. If $\boldsymbol{\theta}$ is constant it is possible to find a least-squares (LS) estimate of $\boldsymbol{\theta}$ by solving the optimization problem

$$\hat{\boldsymbol{\theta}} = \arg\min_{\boldsymbol{\theta}} \left[\boldsymbol{Z} - \boldsymbol{H}\boldsymbol{\theta}\right]^\top \left[\boldsymbol{Z} - \boldsymbol{H}\boldsymbol{\theta}\right]. \tag{14}$$

A solution to (14) exists if $\boldsymbol{\theta}$ observable. This is satisfied if there are sufficiently many heading changes, e.g. if the vehicle follows a square or rectangular trajectory. The stationarity condition on $\boldsymbol{\theta}$ implies that data collected during or immediately after a turn maneuver can not be used in (13). It also implies that the actuator set-points should be similar at every sample time $t_1, t_2, \ldots, t_N$.

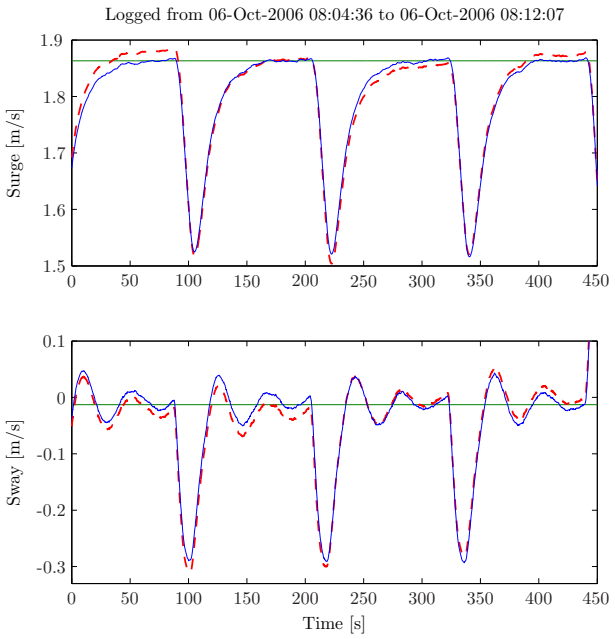

Fig. 2. Current compensation. Dashed and solid curves: before (u and v) and after (u_r and v_r). The solid straight lines are from table-lookups.

If the nature of an experiment renders $\boldsymbol{\theta}$ is unobservable, (13) can not be used. This is for instance the case if the vehicle follows a single straight-line path (e.g. during a 1 DOF surge experiment). An alternative is to use the results from [39], where steady-state maneuvering characteristics for HUGIN 4500 were obtained. In particular, a static table-lookup model for $\boldsymbol{v}_{wb}^b$ was derived, similar to (11). If the output from the table is given as $\hat{\boldsymbol{v}}_{wb}^b$ then it is possible to obtain an estimate of the current from (3), that is,

$$\hat{\boldsymbol{v}}_{mw}^m = \boldsymbol{R}_b^m(\boldsymbol{v}_{mb}^b - \hat{\boldsymbol{v}}_{wb}^b). \tag{15}$$

The velocity $\hat{\boldsymbol{v}}_{wb}^b$ is uncorrelated to $\boldsymbol{R}_b^m$ and $\boldsymbol{v}_{mb}^b$. Note that $\hat{\boldsymbol{v}}_{wb}^b$ is based on steady-state conditions, hence (15) should only be used with similar conditions on $\boldsymbol{R}_b^m$ and $\boldsymbol{v}_{mb}^b$.

The compensation approach can be summarized as:

1) Pick some data for which $\boldsymbol{v}_{wb}^b$ is to be estimated. The start and finish time associated with the data are given as t_0 and t_f, respectively.
2) Select an appropriate subset of the data where the vehicle response has reached steady-state. The start and finish time associated with the subset are given as t_0' and t_f', respectively.
3) For the selected subset, use either (13) or (15) to obtain an estimate of $\boldsymbol{v}_{mw}^m$. Calculate the mean value $\bar{\boldsymbol{v}}_{mw}^m$ and assign it to the time $t' = (t_f' - t_0')/2$.
4) If more than one subset is considered, repeat step 2 and 3 for each subset.
5) If only one subset is considered then $\bar{\boldsymbol{v}}_{mw}^m$ is assumed constant on the time interval $[t_0, t_f]$. Otherwise linear interpolation is used to obtain an estimate of $\boldsymbol{v}_{mw}^m$ on the same interval. The current is assumed to change linearly between each successive pair $(t', \bar{\boldsymbol{v}}_{mw}^m)$.
6) Use the estimate of $\boldsymbol{v}_{mw}^m$, together with $\boldsymbol{R}_m^b$ and $\boldsymbol{v}_{mb}^b$ from the data chosen in step 1 to obtain an estimate of $\boldsymbol{v}_{wb}^b$ on the interval $[t_0, t_f]$. This is done using (3).

Figure 2 shows an example of data before and after current has been compensated for by using (15).

B. Identification Procedure

Since (9) is found to be linear in the plant coefficients (hydrodynamic derivatives) we can rewrite the model by means of a linear regressor $\boldsymbol{\Phi} \in \mathbb{R}^{3\times 19}$ and a parameter vector $\boldsymbol{\varphi} \in \mathbb{R}^{19}$. This yields the equivalent representation

$$\boldsymbol{M}\dot{\boldsymbol{\nu}}_r + \boldsymbol{C}(\boldsymbol{\nu},\boldsymbol{\nu}_r) + \boldsymbol{g}(\boldsymbol{\Theta}) - \boldsymbol{\tau}_P = \boldsymbol{\Phi}(\boldsymbol{\nu},\boldsymbol{\nu}_r)\boldsymbol{\varphi}. \quad (16)$$

The right hand side of (16) is given as

$$\boldsymbol{\Phi}(\boldsymbol{\nu},\boldsymbol{\nu}_r)\boldsymbol{\varphi} = \boldsymbol{\tau}_C - \boldsymbol{d}(\boldsymbol{\nu}_r)\boldsymbol{\nu}_r - l(\boldsymbol{\nu}_r) =: \boldsymbol{F} \quad (17)$$

and the vector of the (unknown) coefficients is defined as

$$\begin{aligned}\boldsymbol{\varphi} = [\, & X_u, X_{|u|u}, X_{vr}, X_{vv}, X_{rr}, X_{\delta\delta uu} \\ & Y_v, Y_r, Y_{|v|v}, Y_{|r|r}, Y_{uv}, Y_{\delta uu}, Y_{\delta ur} \\ & N_v, N_r, N_{|v|v}, N_{|r|r}, N_{uv}, N_{\delta ur}\,]^\top,\end{aligned} \quad (18)$$

where $Y_{uv} = Y_{uv_\delta} + Y_{uv_b}$ and $N_{uv} = N_{uv_\delta} + N_{uv_b}$. From the expression in (17) it trivially follows that

$$[\boldsymbol{\Phi}_{ij}] = \left[\frac{\partial \boldsymbol{F}_i}{\partial \boldsymbol{\varphi}_j}\right], \quad (19)$$

where i and j denote an element in $\boldsymbol{F}$ and $\boldsymbol{\varphi}$, respectively.

With exception of $\boldsymbol{\varphi}$, all the other terms in (16) are assumed known or measured. Reasonable initial conditions for many of the unknown parameters can be found from semi-empirical relationships. With some physical insight in the vehicle hydrodynamics one may also know the lower $\underline{\varphi}$ and upper $\overline{\varphi}$ bounds of the parameters. If this is the case, the bounds can be included in the identification loop. The unknown bounds are usually assigned the values $\pm\infty$.

In summary, the parameter identification task it to estimate the parameter vector $\boldsymbol{\varphi}$ in the continuous-time model structure (16), given observations of the vehicle accelerations, velocities and orientation $(\dot{\boldsymbol{\nu}}_r, \boldsymbol{\nu}_r, \boldsymbol{\nu}, \boldsymbol{\Theta})$, as well as actuator readings $(n, \delta_{r_t}, \delta_{r_b}, \delta_{s_p}, \delta_{s_s})$. Prior to applying the identification algorithm, all the signals must be re-sampled to the non-uniform sampling times t_k, $k = 1, \ldots, N$.

The identification approach used in this paper is is based on the constrained linear least-squares (LS) criteria

$$\begin{aligned}\hat{\boldsymbol{\varphi}} = \arg\min_{\boldsymbol{\varphi}} \sum_{k=1}^{N} [\boldsymbol{y}(t_k) - \boldsymbol{\Phi}(t_k)\boldsymbol{\varphi}]^\top [\boldsymbol{y}(t_k) - \boldsymbol{\Phi}(t_k)\boldsymbol{\varphi}] \\ \text{subject to: } \underline{\boldsymbol{\varphi}} \leqslant \boldsymbol{\varphi} \leqslant \overline{\boldsymbol{\varphi}},\end{aligned} \quad (20)$$

where $\boldsymbol{y}(t_k)$ is the left hand side of (16) at sample k.

Numerous algorithms exist for solving the LS problem formulated above, for which some are available in MATLAB. For a comprehensive treatment on numerical LS methods, the reader is referred to [40]. In some cases the measured data may vary in quality. To model this situation it is possible to include weights in the problem formulation. Typically this is done by incorporating the measurement error covariances. Weights are not included in this paper.

The approach for identifying the model in (10) is analogous to the discussion above, but where $\boldsymbol{\varphi}$ is defined as

$$\boldsymbol{\varphi} = [\, X_u, X_{|u|u}, X_{\delta\delta uu}\,]^\top. \quad (21)$$

The expressions for y and $\boldsymbol{\Phi}$ follows directly from (10).

Note that in addition to the unknown hydrodynamic derivatives in (18) and (21), it is also possible to include constant bias terms (forces or moment) for each degree of freedom. Such additional terms may be necessary in order to remove biases due to unmodeled dynamics, control surface mounting misalignments, and so forth.

Fig. 3. The HUGIN 4500 AUV during sea-trial launch.

IV. Experimental Setup

Navigation data collected by the HUGIN 4500 AUV are used as reference and basis throughout this paper. An overview of vehicle particulars is given subsequently, followed by a description of the experiments conducted in order to identify and validate the models in Section II.

A. Vehicle Specifications

The Kongsberg Maritime manufactured HUGIN 4500 is the latest member of the HUGIN AUV family. Figure 3 shows a picture from one of the trials in September 2006.

The length of the vehicle is approximately 6.5 m and the maximum diameter is 1 m. This gives a nominal dry mass of 1950 kg. Designed for large depths and long endurance, the vehicle can operate at depths down to 4500 meters and operate for 60-70 hours. The nominal cruising speed of the vehicle is about 3.7 knots or 1.9 m/s. The vehicle is passively stable in roll and close to neutrally buoyant.

For propulsion HUGIN 4500 is fitted with a high torque synchronous motor, allowing direct axial drive of a single three-bladed propeller. A cruciform tail configuration with four identical control surfaces is used for maneuvering. The vehicle can operate in either UUV (unmanned underwater vehicle) or AUV mode. In AUV mode the vehicle operates without supervision, and independently of the mother ship. In UUV mode the vehicle is maneuvered close to the mother ship, hence enabling real-time supervision.

HUGIN 4500 is equipped with an inertial navigation system (INS) which calculates position, velocity and attitude using high frequency data from an inertial measurement unit (IMU). Some of the IMU specifications are listed in Table II. In order to obtain a low drift navigation solution, a Kalman filter is implemented which utilizes a variety of navigation sensors for aiding the INS. In UUV mode the surface ship tracks the submersible with an ultra short baseline acoustic position system (USBL). By combining DGPS with USBL, a global position estimate of the AUV can be obtained. This estimate is then sent to the AUV on the acoustic communication link. Additional navigation

TABLE II
IMU SPECIFICATIONS

Model	Gyro Technology	Gyro Bias	Accelerometer Bias
IXSEA IMU90	Fiber optic	$\pm 0.05^\circ$/h	± 500 μg

TABLE III
PRIMARY NAVIGATION AIDING SENSORS

Variable	Sensor	Precision	Rate
Position	Kongsberg HiPAP	Range, Angle: < 20 cm, 0.12°	Varying*
Velocity	RDI WHN 300	$\pm 0.4\,\% \pm 0.2$ cm/s	1 Hz
Pressure	Paroscientific	$0.01\,\%$ full scale	5 Hz

* Data rate is approximately 1/3 Hz. In real-time HUGIN receives position updates at about 1/30 Hz, from the surface vessel via an acoustic link.

sensors include compass, pressure sensor, and Doppler velocity log (DVL). Primary aiding sensors and some of their specifications are listed in Table III. Readers are referred to [41], [42] for additional information on the navigation system and navigation accuracy.

B. Mission Description

During September and October 2006, several sea-trials were conducted with the HUGIN 4500 AUV in the vicinity of 59° 29' N, 10° 28' E, in the Oslo-fjord, Norway. The test area is shown in Fig. 4. More than 60 hours of data were collected, of which approximately 5 hours are utilized in this paper. A brief summary of the data is given below:

1) Suitable data needed for the identification process.
   a) About 1 hour with data resulting from 1 DOF motion where the vehicle was kept at a steady course while varying the propeller rotation rate.
   b) About 1 1/2 hour with data where the vehicle followed square-shaped trajectories. The propeller rotation rate was held fixed throughout the completion of a full square. The sides of the individual squares ranged from 450-600 m in length, sufficient for the vehicle to retain steady-state velocity between 90 degree turns or after changing the propeller rotation rate.
2) Data used for validating the identified models. The trajectories in Fig. 4, marked 1-4, represent the data used for validating the models. Note that this data is independent of the data used during identification.
   a) Data from 1 DOF motion, where the vehicle was kept at a steady course, while varying the propeller rotation rate (marked 1). Not equal to the data used during identification.
   b) Data from zig-zig maneuvers in the horizontal plane (marked 2).
   c) Data gathered while following a traditional lawn mover pattern (marked 3 and 4).

V. Experimental Results

This section reports the experimental evaluation of the identified vehicle models. Since the data used for validation also contain disturbances from current, this effect must be identified and properly accounted for. This is again done using the methods in Section III-A. In the following, various results are presented, succeeded by a discussion on the validity and performance of the models. As can be seen, the response from the models is in general in good agreement with the experimental observations.

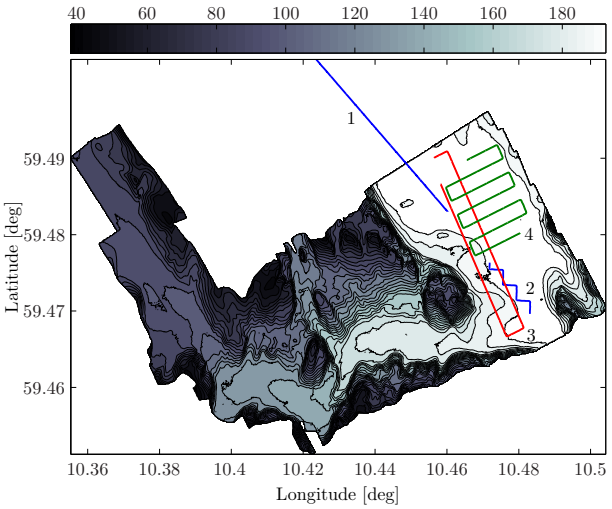

Fig. 4. Test area for the HUGIN AUV. The real trajectories marked 1-4 represent about 2 1/2 hours of data used during the validation stage.

Prior to applying the proposed identification algorithm and the current compensation schemes, the data were wild-point filtered and smoothed in order to enhance accuracy. This was done using the post-processing tool NavLab [43].

A. Model Validation Results

A standard step in system identification to prevent over-fitting observed data, is to validate the model on a new data set not used for estimation. The trajectories of the data used for this particular task are shown in Fig. 4. Each trajectory is associated with a set of actuator signals, which are used as inputs to the models being validated. The model outputs are then checked against the particular trajectory, which is considered as the ground truth. Results from the validation stage in this paper are shown in Table IV-VII, where e is the prediction error of the model. All units are in [m/s]. Some of the data used for compiling these tables are shown in Fig. 5-12. In general, the models show good agreement with the experimental data, and depending on the trajectory, the mean and standard deviations of the prediction errors are in the sub mm/s range, which is respectable.

B. Discussion

So which model is the better? It is important to keep in mind the presumptions that were used when derived the models. The 3 DOF maneuvering model assumes that coupling from heave, pitch and roll can be ignored. Similarly, for the 1 DOF model, all other components than surge are ignored. If the presumptions are violated the model will in general not do the job. As can be seen from Table IV and from Fig. 10, the 1 DOF model performs equally well to the 3 DOF under the condition that the vehicle follows a straight ahead path. For all the other trajectories, the 3 DOF model outperforms the 1 DOF, as it should. Remember that the increased accuracy comes at the cost of an explosion in unknown model coefficients. Usually one has to make a compromise between complexity and accuracy. For some applications the one-step or short-time

prediction of a model is of greater importance than the accuracy of a full batch simulation.

TABLE IV
RESULTS FROM MODEL VALIDATION USING TRAJECTORY 1

Model	State	$\bar{e}$	$\sigma(e)$	$\max(\lvert e_i \rvert)$
1 DOF	u_r	+1.239e-03	+9.676e-03	+2.966e-02
1 DOF*	u_r	+5.949e-03	+8.604e-02	+3.747e-01
3 DOF	u_r	−5.891e-05	+9.875e-03	+3.144e-02
1 DOF*	v_r	+9.315e-04	+8.548e-03	+3.057e-02
3 DOF	v_r	−4.017e-03	+1.019e-02	+2.650e-02

TABLE V
RESULTS FROM MODEL VALIDATION USING TRAJECTORY 2

Model	State	$\bar{e}$	$\sigma(e)$	$\max(\lvert e_i \rvert)$
1 DOF	u_r	+6.341e-02	+9.593e-02	+3.506e-01
1 DOF*	u_r	+7.394e-02	+1.075e-01	+3.869e-01
3 DOF	u_r	+1.094e-03	+1.872e-02	+6.556e-02
1 DOF*	v_r	−1.215e-03	+9.787e-02	+3.113e-01
3 DOF	v_r	−2.811e-04	+1.508e-02	+3.525e-02

TABLE VI
RESULTS FROM MODEL VALIDATION USING TRAJECTORY 3

Model	State	$\bar{e}$	$\sigma(e)$	$\max(\lvert e_i \rvert)$
1 DOF	u_r	+5.270e-03	+3.688e-02	+3.110e-01
1 DOF*	u_r	+7.743e-03	+4.054e-02	+3.523e-01
3 DOF	u_r	−2.594e-03	+6.832e-03	+5.291e-02
1 DOF*	v_r	+3.994e-03	+3.240e-02	+2.802e-01
3 DOF	v_r	−2.049e-03	+8.378e-03	+3.868e-02

TABLE VII
RESULTS FROM MODEL VALIDATION USING TRAJECTORY 4

Model	State	$\bar{e}$	$\sigma(e)$	$\max(\lvert e_i \rvert)$
1 DOF	u_r	+2.195e-02	+6.519e-02	+3.586e-01
1 DOF*	u_r	+2.501e-02	+7.410e-02	+3.947e-01
3 DOF	u_r	−2.798e-03	+1.236e-02	+1.159e-01
1 DOF*	v_r	−6.490e-04	+5.960e-02	+3.228e-01
3 DOF	v_r	−4.095e-03	+1.109e-02	+3.930e-02

VI. Conclusions and Further Work

This paper has reported a step by step procedure for deriving and identifying dynamic models for underwater vehicles. Since the hydrodynamic forces and moments are highly dependent on the water relative velocity of the submersible, it is important that reliable velocity measurements or estimates are obtained prior to the model identification stage. A combination of dedicated experiments and least-squares estimation has been proposed in order to facilitate this task. After establishing the necessary preliminaries, the proposed procedure was used for identifying suitable models for the HUGIN 4500 autonomous vehicle (AUV). The derived models have been extensively cross-validated with uncorrelated data. The vehicle response predicted by the models shows good agreement with real measurements. The work was motivated from the perspective of using the vehicle models for aiding an integrated underwater navigation system.

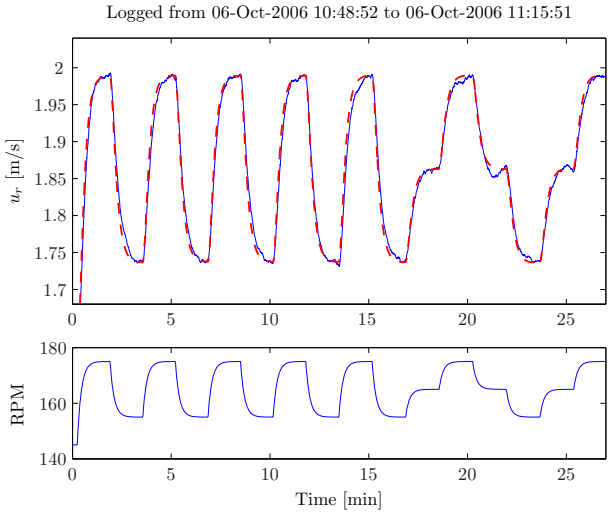

Fig. 5. Data from 1 DOF motion. Solid (blue) lines are the data corresponding to trajectory 1. Dotted (red) line is the output from (10).

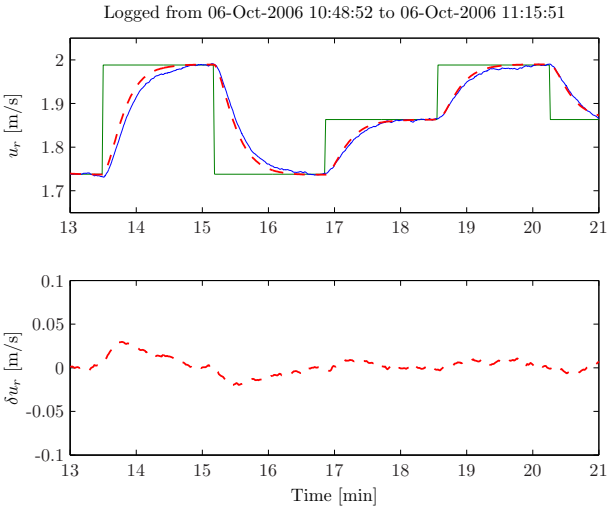

Fig. 6. Data from 1 DOF motion. Solid (blue) line is the data corresponding to trajectory 1. Dotted (red) line in the top plot is the output from (10). The bottom plot shows the prediction error. The staircase (green) is the output from (11).

A. Further Work

Due to the iterative nature of parameter identification, additional parameter tuning will be attempted. Also, in order to facilitate motion in additional degrees of freedom, heave and pitch will be included in the equations of motion.

As the second major step, the possibility of using these mathematical models as means for aiding an integrated underwater navigation system will be studied.

Acknowledgment

The first author acknowledges the financial support from the Research Council of Norway, Kongsberg Maritime, and Kongsberg Defence & Aerospace, through the UNaMap program. Thanks also to the HUGIN engineers and the crew of M/S Simrad Echo for all their help during experiments.

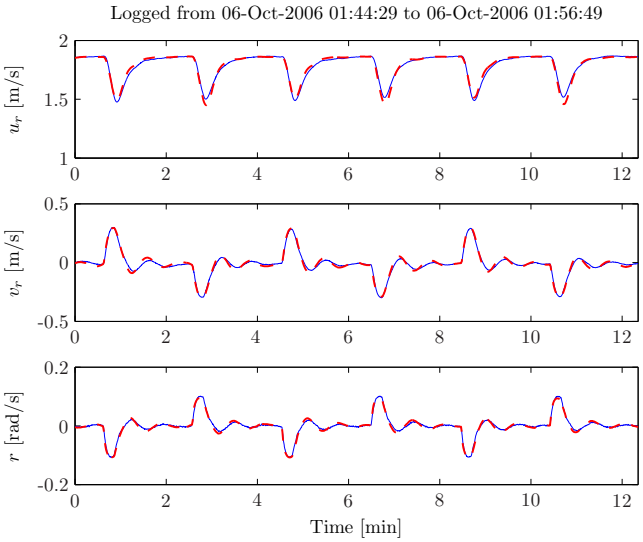

Fig. 7. Data from zig-zag motion. Solid (blue) lines are the data corresponding to trajectory 2. Dotted (red) lines are the output from (9).

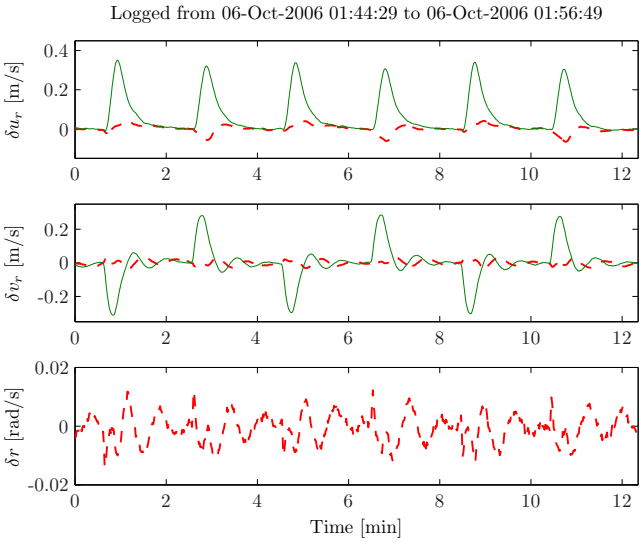

Fig. 8. Data from zig-zag motion. Dotted (red) lines are the prediction errors from (9). Solid (green) is the output from (10) and (11)

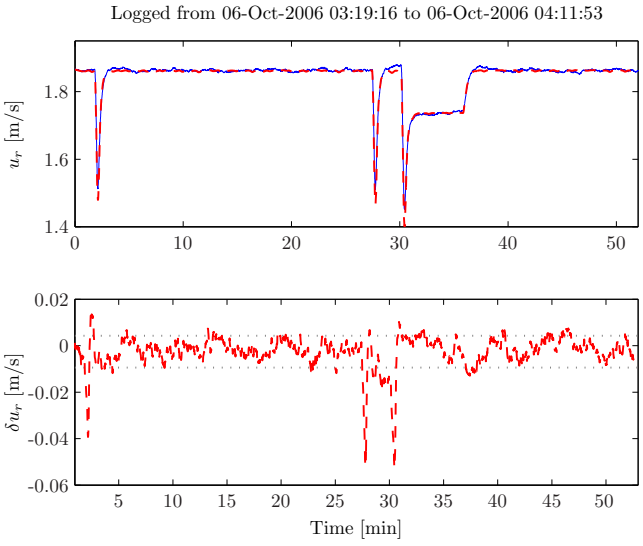

Fig. 9. Data from lawn mower motion. Solid (blue) line is the data corresponding to trajectory 3. Dotted (red) line in the top plot is the output from (9). The bottom plot shows the prediction error.

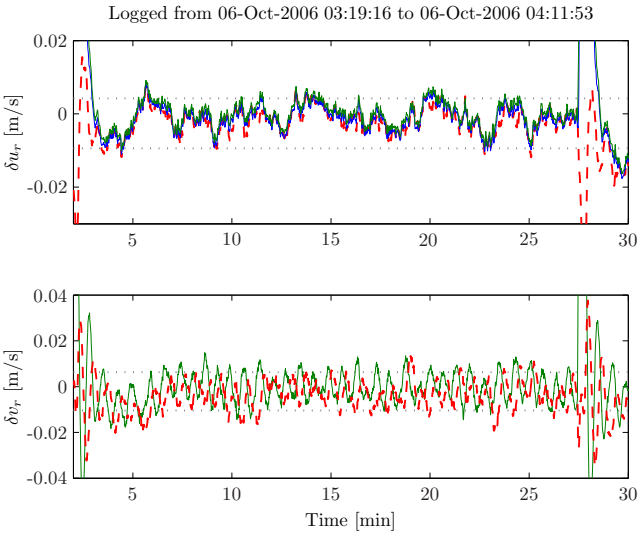

Fig. 10. Data from lawn mower motion. Prediction errors to trajectory 3. Solid (blue) line is the prediction error from (10). Solid (green) lines are the prediction error from (11). Dotted (red) lines are from (9).

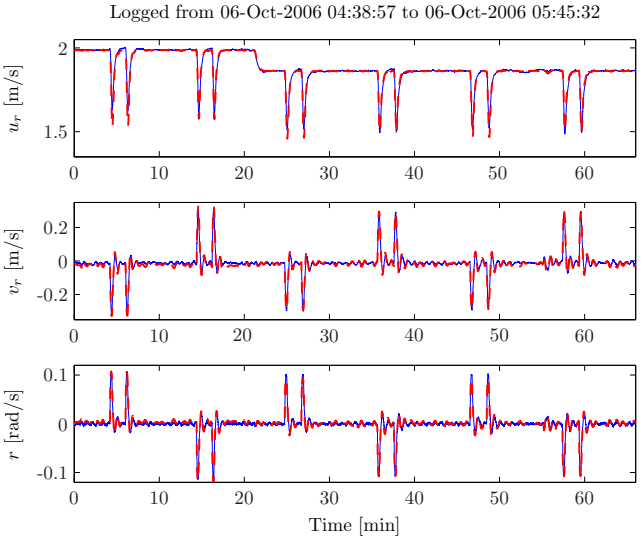

Fig. 11. Data from lawn mower motion. Solid (blue) lines are the data corresponding to trajectory 4. Dotted (red) lines are the output from (9).

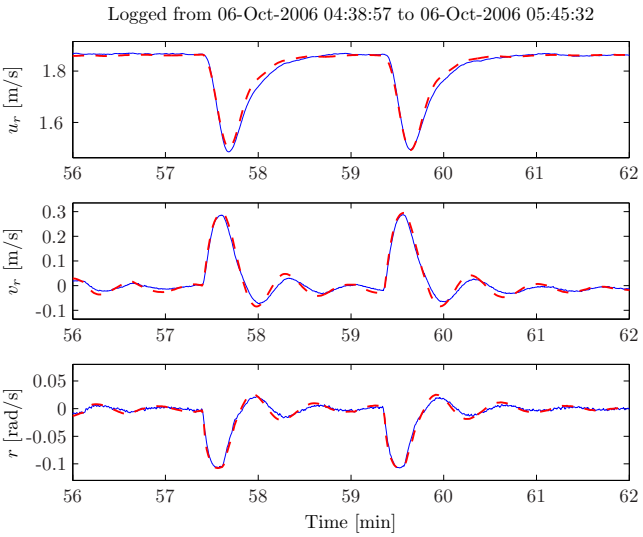

Fig. 12. Data from lawn mower motion. Solid (blue) lines are the data corresponding to trajectory 4. Dotted (red) lines are the output from (9).

REFERENCES

[1] S. H. Lamb, *Hydrodynamics*, 6th ed. Cambridge: University Press, 1932, ISBN 0-521-05515-6.

[2] G. Kirchhoff, "Über die bewegung eines rotationskörpers in einer flüssigkeit," *Crelle's Journal*, no. 71, pp. 237–273, 1869, (In German).

[3] F. Imlay, "The complete expressions for "added mass" of a rigid body moving in ideal fluid," David Taylor Model Basin, Washington D.C., Tech. Rep. DTMB 1528, 1961.

[4] K. S. M. Davidson and L. I. Schiff, "Turning and course keeping qualities," *Transactions of the Society of Naval Architects and Marine Engineers (SNAME)*, vol. 54, pp. 152–200, 1946.

[5] M. A. Abkowitz, "Lectures on ship hydrodynamics - steering and manoeuvrability," Hydro- and Aerodynamics Laboratory, Lyngby, Denmark, Tech. Rep. Hy-5, May 1964.

[6] D. Clarke, "The foundations of steering and manoeuvring," in *Proceedings of 6th Conference on Maneuvering and Control of Marine Craft (MCMC 2003)*, Girona, Spain, September 2003.

[7] G. H. Bryan, *Stability in aviation : an introduction to dynamical stability as applied to the motions of aeroplanes*. London: Macmillan, 1911.

[8] K. K. Fedyaevsky and G. V. Sobolev, *Control and Stability in Ship Design*. Leningrad: State Union Shipbuilding Publishing House, 1963.

[9] T. I. Fossen, *Guidance and Control of Ocean Vehicles*. Chichester, UK: John Wiley & Sons Ltd, 1994, ISBN 0-471-94113-1.

[10] ——, *Marine Control Systems : Guidance, Navigation and Control of Ships, Rigs and Underwater Vehicles*. Trondheim, Norway: Marine Cybernetics, 2002, ISBN 82-92356-00-2.

[11] R. Skjetne, "The maneuvering problem," Ph.D. dissertation, Norwegian University of Science and Technology, Trondheim, Norway, 2005, ISBN 82-471-6861-8.

[12] M. Gertler and S. C. Hagen, "Standard equations of motion for submarine simulations," Naval Ship Research and Development Center, Washington D.C., Tech. Rep. DTMB 2501, 1967.

[13] J. Feldman, "DTMSRDC revised standard submarine equations of motion," Naval Ship Research and Development Center, Washington D.C., Tech. Rep. DTNSRDC-SPD-0393-09, 1979.

[14] H. N. Arafat, D. J. Stilwell, and W. L. Neu, "Development of a dynamic model of a small high-speed autonomous underwater vehicle," in *OCEANS '06. 'Revolutionizing Marine Science & Technology'. Proceedings*, Boston, MA, September 2006.

[15] J. Evans and M. Nahon, "Dynamics modeling and performance evaluation of an autonomous underwater vehicle," *Ocean Engineering*, vol. 31, no. 14, pp. 1835–1858, October 2004.

[16] M. Nahon, "A simplified dynamics model for autonomous underwater vehicles," in *Autonomous Underwater Vehicle Technology, 1996. AUV '96., Proceedings of the 1996 Symposium on*, Monterey, CA, 1996, pp. 373–379.

[17] M. A. Abkowitz, "Stability and Motion Control of Ocean Vehicles," MIT, Massachusetts, Tech. Rep. Sea Grant Project GH-1, May 1969.

[18] C. L. Crane, H. Eda, and A. Landsburg, "Motions in waves and controllability," in *Principles of Naval Architecture*, E. V. Lewis, Ed. Jersey City, NJ: Society of Naval Architects and Marine Engineers, 1988, vol. 3, ISBN 0-939773-02-3.

[19] P. Mandel, *Resistance, Propulsion and Vibration*, ser. Principles of Naval Architecture, J. P. Comstock, Ed. New York, NY: Society of Naval Architects and Marine Engineers, 1977.

[20] D. A. Smallwood, "Advances in dynamical modeling and control of underwater robotic vehicles," Ph.D. dissertation, Johns Hopkins University, 2003.

[21] A. Sørensen, "Lecture notes: Marine cybernetics - modeling and control," 2005, report UK-05-76, Department of Marine Technology, Norwegian University of Science and Technology.

[22] B. Jalving, "The NDRE-AUV flight control system," *IEEE Journal of Oceanic Engineering*, vol. 19, no. 4, pp. 497–501, Oct. 1994.

[23] J. Kim, K. Kim, H. Choi, W. Seong, and K.-Y. Lee, "Depth and heading control for autonomous underwater vehicle using estimated hydrodynamic coefficients," in *OCEANS, 2001. MTS/IEEE Conference and Exhibition*, vol. 1, Honolulu, HI, 2001, pp. 429–435.

[24] D. A. Smallwood and L. L. Whitcomb, "Model-based dynamic positioning of underwater robotic vehicles: theory and experiment," *IEEE Journal of Oceanic Engineering*, vol. 29, no. 1, pp. 169–86, Jan. 2004.

[25] J. E. Refsnes, A. J. Sørensen, and K. Y. Pettersen, "Design of output-feedback control system for high speed maneuvering of an underwater vehicle," in *OCEANS 2005*, Washington, DC, USA, 2005, pp. 1167–74.

[26] A. Alessandri, M. Caccia, and G. Veruggio, "Fault detection of actuator faults in unmanned underwater vehicles," *Control Engineering Practice*, vol. 7, no. 3, pp. 357–68, Mar. 1999.

[27] G. Antonelli, "A survey of fault detection/tolerance strategies for auvs and rovs," in *Fault Diagnosis and Fault Tolerance for Mechatronic Systems: Recent Advances*, ser. Springer Tracts in Advanced Robotic. Springer-Verlag Berlin Heidelberg, 2003, vol. 1, pp. 109–127, ISBN 978-3-540-44159-5.

[28] L. Ni and C. Fuller, "Control reconfiguration based on hierarchical fault detection and identification for unmanned underwater vehicles," *Journal of Vibration and Control*, vol. 9, no. 7, pp. 735–48, July 2003.

[29] K. M. Fauske, Ø. Hegrenæs, F. Gustafsson, and O. Hallingstad, "Model-based methods for fault detection and filtering in underwater navigation systems," in *OCEANS Europe*, Aberdeen, 2007, to appear.

[30] J. C. Kinsey and L. L. Whitcomb, "Model-based nonlinear observers for underwater vehicle navigation: Theory and preliminary experiments," in *Proceedings - IEEE International Conference on Robotics and Automation*, April 2007, to appear.

[31] J. E. Refsnes, K. Y. Pettersen, and A. J. Sørensen, "Observer design for underwater vehicles with position and angle measurement," in *Proceedings of 7th Conference on Maneuvering and Control of Marine Craft (MCMC 2006)*, Lisboa, 2006.

[32] O. Egeland and J. T. Gravdahl, *Modeling and Simulation for Automatic Control*. Trondheim, Norway: Marine Cybernetics, 2002, ISBN 82-92356-01-0.

[33] SNAME, "Numenclature for treating the motion of a submerged body through a fluid," The Society of Naval Architects and Marine Engineers, Tech. Rep. Technical and Research Bullitin No. 1-5, 1950.

[34] M. Blanke, K.-P. Lindegaard, and T. Fossen, "Dynamic model for thrust generation of marine propellers," in *Proceedings of 5th Conference on Maneuvering and Control of Marine Craft (MCMC 2000)*, Aalborg, Denmark, 2000, pp. 363–8.

[35] J. Kim and W. K. Chung, "Accurate and practical thruster modeling for underwater vehicles," *Ocean Engineering*, vol. 33, no. 5, pp. 566–586, Apr. 2006.

[36] L. L. Whitcomb and D. R. Yoerger, "Development, comparison, and preliminary experimental validation of nonlinear dynamic thruster models," *IEEE Journal of Oceanic Engineering*, vol. 24, no. 4, pp. 481–494, 1999.

[37] R. D. Finck and D. E. Hoak, *USAF Stability and Control DATCOM*, Wright-Patterson Airforce Base, Ohio, April 1978.

[38] S. F. Hoerner and H. V. Borst, *Fluid-Dynamic Lift : Practical Information on Aerodynamic and Hydrodynamic Lift*. New Jersey: Hoerner Fluid Dynamics, 1975.

[39] Ø. Hegrenæs, O. Hallingstad, and B. Jalving, "A framework for obtaining steady-state maneuvering characteristics of underwater vehicles using sea-trial data," in *15th Mediterranean Conference on Control and Automation (MED'07)*, Athens, 2007, sumitted.

[40] Å. Björck, *Numerical methods for least squares problems*. Philadelphia: SIAM, 1996, ISBN 0-89871-360-9.

[41] B. Jalving, K. Gade, O. Hagen, and K. Vestgård, "A toolbox of aiding techniques for the HUGIN AUV integrated inertial navigation system," in *OCEANS 2003, Proceedings*, vol. 2, San Diego, CA, USA, 2003, pp. 1146–1153.

[42] B. Jalving, K. Vestgård, and N. Størkersen, "Detailed seabed surveys with AUVs," in *Technology and Applications of Autonomous Underwater Vehicles*, G. Griffiths, Ed. London: Taylor & Francis, 2003, vol. 2, pp. 179–201, ISBN 0-415-30154-8.

[43] K. Gade, "NavLab, a generic simulation and post-processing tool for navigation," *European Journal of Navigation*, vol. 2, no. 4, pp. 21–59, Nov. 2004.